CrystEngComm

ROYAL SOCIETY OF CHEMISTRY

HIGHLIGHT

View Article Online
View Journal | View Issue

Cite this: *CrystEngComm*, 2026, **28**, 1453

Crystallization, replacement, and redox pathways governing rare earth carbonate and phosphate formation

Juan Diego Rodriguez-Blanco, *[a] Melanie Maddin, †[b] Remi Rateau, †[b] Adrienn Maria Szucs, †[b] Luca Terribili, †[b] Beatriz Vallina†[c] and Kristina Petra Zubovic [b]

Rare earth elements are critical raw materials for modern technologies and the global shift toward sustainable energy. Yet, their extraction and separation remain environmentally challenging due to complex geochemical behavior and limited understanding of mineral formation mechanisms. This study integrates recent experimental advances to elucidate the fundamental processes controlling the crystallization and transformation of REE-bearing carbonates and phosphates. REE carbonate formation from aqueous solutions follows a non-classical pathway involving amorphous precursors and metastable intermediates that gradually transform into stable hydroxycarbonates such as kozoite and bastnäsite. The kinetics, polymorph selection, and resulting morphologies are governed by the ionic potentials of the REE^{3+} cations, temperature, and dehydration dynamics. Mineral replacement reactions between REE-bearing fluids and common host minerals like carbonates (calcite, aragonite, dolomite, siderite) and phosphates (vivianite), proceed through coupled dissolution–precipitation, producing pseudomorphic textures. The extent and texture of these transformations are controlled by epitaxial relationships, porosity generation, and local equilibrium conditions. Redox-driven processes, particularly Ce^{3+}–Ce^{4+} and Fe^{2+}–Fe^{3+} oxidation in siderite and vivianite, promote formation of secondary oxides (cerianite, hematite) that influence REE mobility and sequestration. In fluorine-bearing environments, transient fluocerite stabilizes and subsequently transforms epitaxially into bastnäsite, demonstrating the chemical and structural controls governing ore mineralization. Finally, we explore sustainable REE recovery using waste-derived sorbents such as eggshell calcite. Experiments show temperature-dependent REE uptake and complex phase transformations, offering insights for circular-economy approaches to resource recycling. Collectively, these results establish a unified mechanistic framework linking REE mineral formation, transformation, and recovery. By bridging natural ore-forming processes with green chemistry strategies, this study advances understanding of REE geochemistry and supports the development of environmentally sustainable extraction and recycling technologies.

Received 14th November 2025,
Accepted 30th January 2026

DOI: 10.1039/d5ce01083g

rsc.li/crystengcomm

1. Introduction

Rare earth elements (REEs), encompassing the 15 lanthanides, are fundamental strategic raw materials critical to modern civilization and the transition to a sustainable future.[1] Their unique optical, magnetic, and catalytic properties make them indispensable components in a vast array of high-technology devices, including mobile phones, computers, catalysts, and permanent magnets.[2] They are the pillar of green energy technologies; electric vehicles, solar cells, and generators of wind turbines all require significant quantities of REEs.[3] This essential role has led to a continuously growing global demand, placing immense pressure on mining industries to secure supply chains.

Despite their name, REEs are relatively abundant in the Earth's crust, with minable concentrations being the primary limitation. Natural REE abundances are strongly influenced by the odd–even atomic number effect described by Harkins' rule, resulting in the characteristic sawtooth patterns of REE distributions in geological materials.[1] Crystallisation and geochemical processes can reshape how primary REE abundance patterns are expressed in mineral systems, leading to local fractionation effects and characteristic anomalies during mineral growth and replacement.

[a] *iCRAG, Department of Geology, School of Natural Sciences, Trinity College Dublin, Dublin 2, Ireland. E-mail: J.D.Rodriguez-Blanco@tcd.ie*
[b] *Department of Geology, School of Natural Sciences, Trinity College Dublin, Dublin 2, Ireland*
[c] *School of Chemistry, Trinity College Dublin, Dublin 2, Ireland*
† These authors contributed equally to this work.

The global REE landscape is dominated by China, which has supplied over 80% of the world's REEs during the last decades, creating geopolitical concerns and market volatility.[1] While other countries like Australia, Russia, India, Brazil, and Vietnam hold significant reserves, the concentration of processing capacity in China underscores a critical supply risk. This imbalance is exacerbated by the fact that natural deposits rarely contain REEs in the exact ratios required by modern technology; for instance, high-demand elements like Dy and Nd are often less abundant in ores than lower-demand LREEs like Ce and La. This disconnection between natural occurrence and market needs, often termed the "rare earth crisis", fuels the urgency for finding new deposits, improving recycling, and understanding ore formation to optimize processing.[4]

The challenges extend beyond geopolitics and mineralogy to the very chemistry of REEs. The chemical similarity of the lanthanides arises from the effective shielding of their 4f electrons, which do not participate strongly in bonding. This shielding effect leads to the systematic decrease in ionic radii across the series known as the lanthanide contraction.[5] Conventional separation techniques rely on thousands of stages of solvent extraction, a process that is not only energy-intensive but also generates vast quantities of toxic and radioactive waste.[5] This environmental footprint poses a significant societal challenge and contradicts the green ideals of the technologies they enable. Therefore, any advancement in understanding the natural processes that fractionate REEs, such as their preferential partitioning into specific minerals during crystallization or their differential mobility in hydrothermal fluids, can provide foundational insights for developing cleaner, more efficient industrial separation methods.

The primary economic sources of REEs are carbonatites and associated alkaline igneous rocks, which host minerals like bastnäsite ($REECO_3F$), monazite ($REEPO_4$), and xenotime (YPO_4).[6] These deposits are magmatic or hydrothermal in origin and are typically enriched in light REEs (LREEs: La, Ce, Pr, Nd), while heavy REEs (HREEs: *e.g.*, Tb, Dy, Ho) are less abundant but often more critical. The formation of these deposits is a complex interplay of magmatic and hydrothermal processes, where fluids rich in ligands like F^-, Cl^-, and SO_4^{2-} mobilize, transport, and ultimately precipitate REEs into economic concentrations.[7–9] Key minerals in this paragenetic sequence can include fluocerite ($REEF_3$),[10] hypothesized as a precursor to fluorocarbonates and cerianite (CeO_2),[11] though its formation pathways remain poorly constrained.

Beyond primary deposits, secondary sources formed by weathering (such as laterites, bauxites, and placer deposits) offer alternative resources. Furthermore, the pressing need to diversify supply has catalyzed research into unconventional and secondary sources. These include the recycling of electronic waste (e-waste), of which less than 20% is currently recycled, as well as the potential extraction of REEs from coal fly ash, sedimentary phosphate deposits, deep-sea sediments, and iron phosphate ores.[12] For example, the recent discovery of a major REE-phosphate deposit associated with apatite in the Kiruna iron mine, Sweden, highlights the growing importance of understanding the genetic link between phosphorous, iron, and REE mineralization. Effectively harnessing these alternative resources requires a deep geochemical understanding of how REEs are hosted, released, and could be re-concentrated within these complex matrices.

A major impediment to more efficient exploration and exploitation across all deposit types is a fundamental lack of understanding of the physicochemical conditions that govern REE mobility and mineral crystallization mechanisms. A substantial body of experimental and spectroscopic work[82–86] has established that the interaction of REEs with carbonate and phosphate minerals such as calcite, vaterite, and monazite is dominated by lattice and near-surface incorporation processes rather than classical surface sorption. Studies combining EXAFS, TRLFS, AFM, and diffraction methods have shown that trivalent REEs substitute for Ca^{2+} in calcite and vaterite, often inducing local structural distortions, modified coordination environments, and specific charge-compensation mechanisms, particularly for the larger light REEs. Incorporation has been demonstrated to occur not only during crystal growth, but also under recrystallization and polymorphic phase-transformation conditions, such as the vaterite-to-calcite transition, which proceeds *via* coupled dissolution–reprecipitation pathways and results in full transfer of incorporated REEs into the newly formed phase. These studies further highlight the strong influence of solution chemistry (*e.g.*, alkali ions, nitrate) on incorporation kinetics, defect formation, and retention efficiency. Together, this work provides an atomistic and thermodynamic foundation for understanding REE solid-solution formation in carbonate systems. However, the crystallization pathways of REE-carbonates like bastnäsite are known to involve complex, multi-step dehydration sequences and metastable intermediates, processes highly sensitive to temperature, fluid chemistry, and ionic radii.[13] Similarly, the roles of host carbonate minerals like calcite, dolomite, aragonite, siderite, and phosphates like apatite, vivianite in recrystallization and replacement reactions during hydrothermal and metasomatic events are key to understanding ore genesis but are not fully elucidated.

This review paper therefore aims to analyze the current state of knowledge on the fundamental mechanisms controlling the formation of REE-bearing minerals, with a particular focus on carbonates. We will address the precise crystallization pathways from aqueous solution, examining the sequence from amorphous precursors through metastable phases to the stable bastnäsite. Furthermore, we will explore the factors affecting the kinetics and mechanisms of mineral replacement reactions, where common crustal minerals such as calcite, dolomite, and siderite are transformed into REE ore minerals through fluid–rock interactions. By integrating insights from

experimental studies of these processes under well-controlled hydrothermal conditions, we seek, in the long-term, to build a unified model that clarifies the complex paragenetic sequences observed in natural deposits. This fundamental understanding is critical for developing predictive exploration models, optimizing mineral processing and REE separation techniques, and innovating new recycling methodologies to secure a sustainable supply of these critical elements.

To investigate these processes, our experimental program has followed a bottom-up approach, gradually increasing system complexity. We first studied the crystallization of REE-carbonates from simple solutions containing only CO_3^{2-} and REE^{3+}. We then examined how trace REEs influence $CaCO_3$ crystallization, revealing their role during nucleation and growth. Building on these results, we explored replacement reactions in which REE-bearing fluids interact with common carbonate minerals (*i.e.*, calcite, aragonite, dolomite), considering both single- and multi-REE systems. Finally, we extended our experiments to more complex scenarios, including replacement reactions coupled to redox transformations and the influence of additional ligands such as fluorine, an element commonly associated with bastnäsite, that may open alternative reaction pathways. Together, this experimental work provides a mechanistic framework for understanding how REEs interact with carbonate and phosphate hosts across increasing levels of complexity, thereby establishing the basis for developing sustainable, green chemistry strategies for their recovery and recycling.

2. Crystallization from solution: general pathways and mechanisms

Precipitation of REE carbonates from solution underpins many extraction and separation processes. Detailed knowledge of the kinetics and intermediate metastable phases enables more efficient recovery, selective fractionation of REEs, and tailoring of particle morphologies for advanced applications in catalysts, ceramics, magnets, and optical materials.

The crystallization of REE carbonates from aqueous solution follows a consistent non-classical pathway dominated by the initial precipitation of metastable amorphous precursors.[14–16] These nanoscale, hydrous phases (general formula $REE_2(CO_3)_3{\cdot}xH_2O$, where $x \approx 4$–5) form instantaneously upon mixing REE^{3+} and CO_3^{2-}-bearing solutions under high supersaturation conditions (Fig. 1), similarly to Ca–Mg carbonates.[17–22] The subsequent transformation kinetics and selected crystallization pathways are principally governed by two factors: the ionic potential (charge density, Z/r) of the specific REE^{3+} cation and the reaction temperature.

Transformation proceeds through a series of dehydration and crystallization steps. At lower temperatures (≤60 °C), the amorphous precursor typically crystallizes into hydrated phases, most commonly the octahydrate lanthanite-type structure ($REE_2(CO_3)_3{\cdot}8H_2O$) or a lower hydrate tengerite-type structure ($REE_2(CO_3)_3{\cdot}2\text{-}3H_2O$).[13–16,23] The stability of these

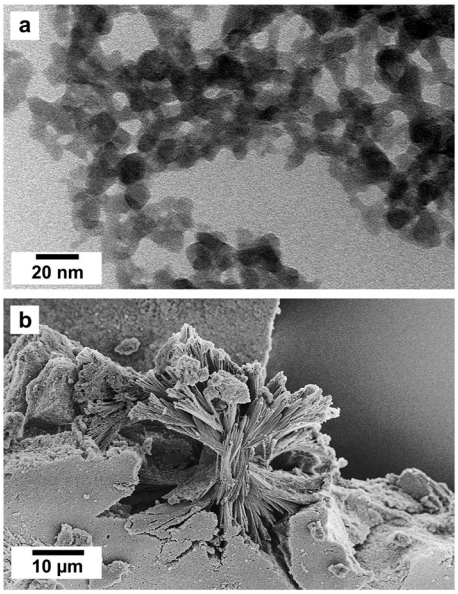

Fig. 1 (a) Transmission electron microscopy image of amorphous Nd carbonate consisting of hydrated nanoparticles formed directly from aqueous solution upon mixing CO_3^{2-}- and Nd^{3+}-bearing aqueous solutions. (b) Spherulitic Nd-kozoite produced by transformation of the amorphous Nd carbonate. The surrounding massive material consists of amorphous Nd carbonate.

hydrated crystalline phases decreases with increasing temperature. Under hydrothermal conditions ($T \geq 95$ °C), the system evolves toward anhydrous hydroxycarbonates, primarily the orthorhombic polymorph $REECO_3(OH)$ (kozoite; Fig. 1) and its hexagonal dimorph $REECO_3(OH)$ (hydroxylbastnäsite),[13–16] *via* progressive dehydration and dissolution–reprecipitation reactions.

The crystallization of these solids from solution is often characterized by two different processes: spherulitic growth

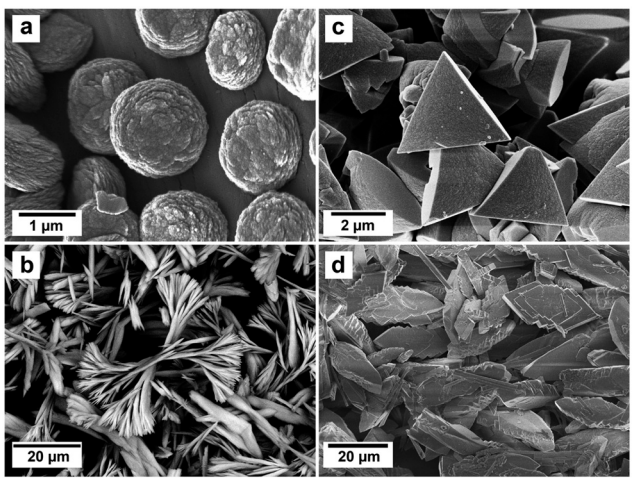

Fig. 2 Spherulitic growth of (a) La-kozoite after La-lanthanite at 21 °C; (b) Pr-kozoite at 35 °C crystallised directly from an amorphous Pr carbonate; (c) La-hydroxylbastnasite formed after La-kozoite *via* dissolution–recrystallisation; (d) Dy-kozoite formed after Dy-tengerite *via* dissolution–recrystallisation.

and coupled dissolution–recrystallisation (Fig. 2). Both transformation mechanisms are strongly governed by the difference in solubility products (K_{sp}) between the reactant and the product. For example, amorphous precursors, being highly disordered and hydrated, usually have a significantly higher solubility than its crystalline counterparts.[16] A large ΔK_{sp} ($K_{sp\ amorphous} \ggg K_{sp\ crystalline}$) creates a strong driving force for rapid transformation. When this difference is maximized, typically under conditions that induce fast precursor breakdown (*e.g.*, high temperature, rapid heating rate), the localized release of ions generates extreme supersaturation with respect to the crystalline phase. This promotes non-equilibrium spherulitic growth *via* continuous nucleation at advancing growth fronts.[15,16,18–24]

Spherulitic growth is a nucleation-driven growth mechanism that results in spherical or dumbbell-shaped polycrystalline nanoaggregates[24] (Fig. 1b and 2a and b). It is usually initiated by the rapid dissolution of the amorphous precursor[16–25] or crystalline hydrated phases like lanthanite.[13–16] The predominance of this mechanism during REE-carbonate crystallization is intrinsically linked to the stability and dissolution kinetics of the initial amorphous phase, which are governed by the dehydration energy of the REE^{3+} ion and, in turn, by its ionic potential.[26–28] This trend is further reinforced by a gradual reduction in hydration coordination number from 9 to 8, which produces more compact and rigid hydration shells in the heavier REEs, slowing water-exchange kinetics, and enhancing the kinetic stabilization of amorphous and weakly hydrated intermediates. The overall progression from a disordered, hydrated solid to a crystalline carbonate is thus a function of competing factors: the rate of water loss from the coordination sphere of the REE^{3+} ion *versus* the rate of ion reorganization into a more thermodynamically stable crystalline phase. Heavier REEs, with their higher ionic potentials and stronger hydration shells, form longer-lived amorphous and intermediate phases and therefore require more energetic conditions (higher temperatures) or longer reaction times to crystallize into anhydrous end members compared with lighter REEs.[14–16] The rate of heating can also result in quicker approach to the supersaturation level required to promote non-equilibrium nucleation-driven processes.[15] As a result, the final structure and morphology of the crystalline product are not intrinsic properties of the mineral phase alone but are dictated by the dehydration kinetics of the precursor. The rate at which water is released governs the evolution of supersaturation, thereby controlling whether crystallization proceeds *via* classical growth or through spherulitic growth. Residual water remaining around the REE^{3+} cation due to incomplete dehydration can enter into the crystalline structure, influencing not only morphology but also polymorph selection, and may even affect the stability of REE oxides formed at high temperatures after decarbonation. Experimental work[29] demonstrated that heavier REEs can even retain part of their original hydration shells up to temperatures close to 1000 °C.

When the solubility difference (ΔK_{sp}) between reactant and product phases is small, as typically occurs during transformations between crystalline intermediates of comparable stability (*e.g.*, transformation of kozoite to hydroxylbastnäsite), the thermodynamic driving force is lower and reaction kinetics are slow. Under these circumstances and similarly to the vaterite–calcite transformation in the $CaCO_3$ system,[17,18,22] dissolution–reprecipitation becomes the dominant transformation mechanism. This process involves the progressive dissolution of the metastable phase into solution, followed by the heterogeneous nucleation and growth of the more stable, less soluble phase. The interface-controlled nature of this mechanism promotes gradual equilibration, with ion-by-ion addition to crystal surfaces facilitating Ostwald ripening and the development of large, well-faceted, euhedral morphologies[17] (Fig. 2c and d).

2.1. Effect of REE during the crystallisation from solution of $CaCO_3$

Recent experimental work has shown that REE also strongly influence the early stages of $CaCO_3$ formation. Terribili *et al.* (2024)[30] demonstrated that the presence of REE^{3+} ions slows down nucleation and growth kinetics of $CaCO_3$, with the degree of inhibition scaling with both concentration and ionic potential (Fig. 3). At high concentrations of heavier REEs, poorly ordered REE–Ca-carbonate precursors were detected before the crystallization of calcite and vaterite, similarly to the highly hydrated amorphous phases observed by Vallina *et al.* (2015).[16] These precursors, consisting of nanometer-sized spheres, temporarily reduce the effective concentration of Ca^{2+}, CO_3^{2-}, and REE^{3+} in solution, thereby lowering supersaturation levels and affecting the subsequent crystallization kinetics. Their transient stability highlights a nonclassical crystallization pathway,[31] where amorphous phases can play a decisive role in dictating the kinetics and polymorph outcome.

Results show that REEs inhibit the formation of calcite and favor vaterite relative to the pure system (Fig. 4). While vaterite maintained its usual spherulitic morphology (Fig. 4a), it developed surface defects (roughness, pits, and imperfections) that became more pronounced with increasing REE concentrations and atomic mass. Calcite, by contrast, showed much stronger morphological modifications (Fig. 4b and c). Instead of well-formed rhombohedra, it often exhibited irregular surfaces, edge and corner distortions, and nanodomain textures on the (104) face. These features could be attributed to preferential adsorption of REE^{3+} ions on specific crystallographic sites and subsequent structural incorporation,[32] which locally inhibit growth and generate nonclassical architectures.[33] Together, these observations suggest that REEs act both by stabilizing amorphous intermediates and by perturbing classical crystal growth, ultimately reducing crystallization rates and producing crystals with complex morphologies. During subsequent transformation to calcite, REEs would be redistributed *via*

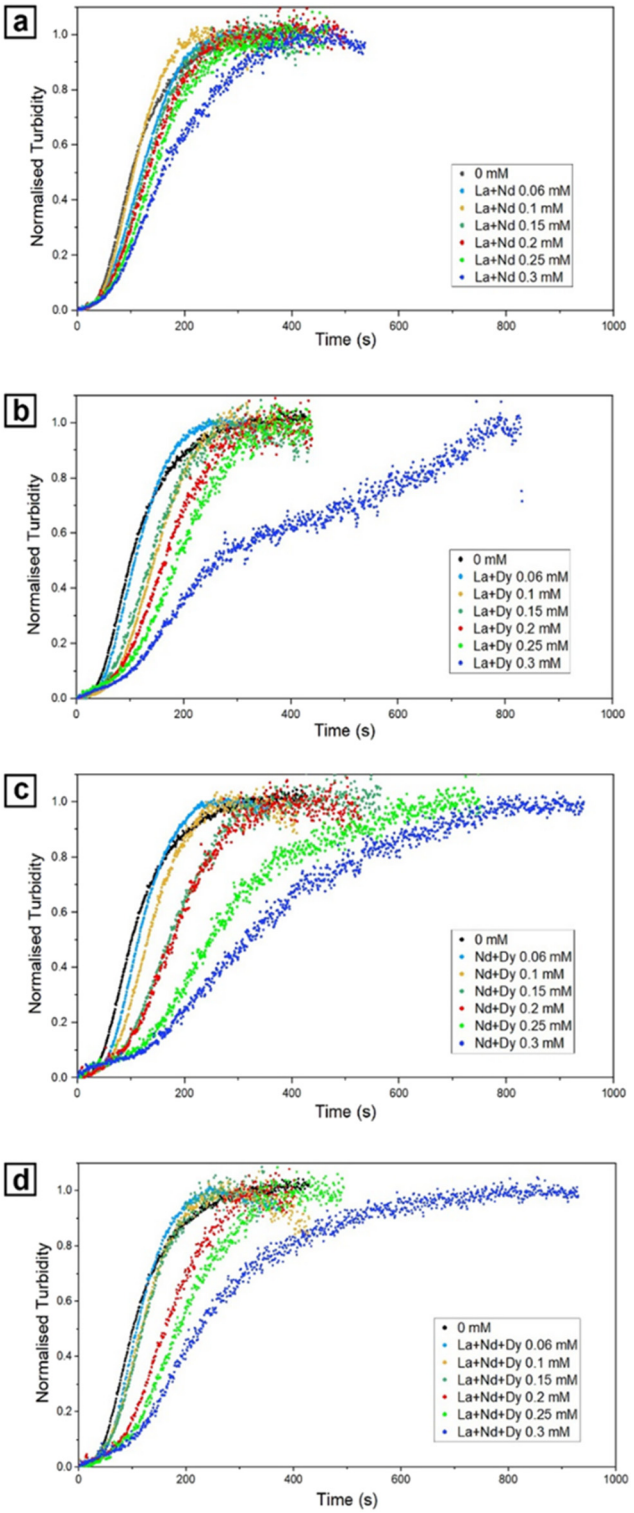

Fig. 3 Normalized turbidity graphs obtained using UV-Vis spectrophotometry showing the effect of multiple REEs during the crystallization of $CaCO_3$. The graphs show (a) the $CaCO_3$ system with La + Nd, (b) La + Dy, (c) Nd + Dy, and (d) La + Nd + Dy. All REEs solutions have equimolar concentrations, with total combined concentrations of REEs ranging from 0 to 0.3 mM.

coupled dissolution–reprecipitation processes, consistent with previous observations for Eu-bearing systems.[34]

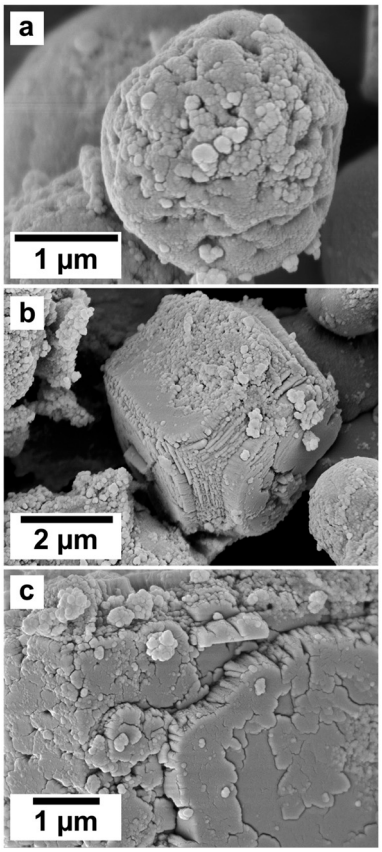

Fig. 4 SEM images of (a) vaterite crystallized in the presence of REEs (La + Nd + Dy 0.06 mM) showing high surface roughness. (b) Surface of calcite crystals (La + Nd + Dy 0.3 mM); (c) details of calcite (104) face obtained in the La + Nd + Dy 0.3 mM experiments.

3. Interaction of REEs with Ca–Mg–Fe carbonates

In hydrothermal environments, the mobility, concentration, and eventual mineralization of REEs are strongly influenced by their interactions with Ca–Mg–Fe carbonate minerals (*e.g.*, calcite, aragonite, dolomite, siderite).[35] These reactions commonly proceed *via* coupled dissolution–precipitation, with successive generations of REE carbonates and phosphates evolving toward increasingly stable assemblages as fluid–rock equilibration progresses. Such experimental findings carry important implications for natural systems, offering valuable insights into the mechanisms that govern the formation of economic REE deposits, particularly hydrothermal carbonatites where bastnäsite represents the principal ore mineral.

3.1. Mineral replacement reactions in REE–Ca–Mg-carbonate systems

The hydrothermal interaction between REE-bearing aqueous solutions and common Ca–Mg carbonate minerals (calcite, aragonite, dolomite) is translated into a complex, multi-stage mineralization process characterized by pseudomorphic

replacements (Fig. 5 and 6). The general reaction pathway is fundamentally governed by dissolution–precipitation mechanisms, where the host carbonate dissolves, increasing the local concentration of CO_3^{2-} ions at the fluid-mineral interface, increasing supersaturation levels and promoting the crystallization of less-soluble REE-bearing carbonate phases.[36–38] The replacement proceeds centripetally, *i.e.*, from the grain periphery inward (Fig. 6), often preserving the original morphology of the host crystal while completely transforming its composition.

A key finding across these studies is the consistent, temperature-dependent crystallization sequence observed for light REEs (La, Pr, Nd): lanthanite [$REE_2(CO_3)_3{\cdot}8H_2O$] → kozoite [orthorhombic $REECO_3(OH)$] → hydroxylbastnäsite [hexagonal $REECO_3(OH)$][36–38] (Fig. 7). This progression reflects a pathway of increasing thermodynamic stability and dehydration. The ionic radius of the REE^{3+} cation exerts a primary control on polymorph selection. Larger ions (La^{3+}, Pr^{3+}, Nd^{3+}) readily facilitate this full sequence, while smaller, heavier REEs like Dy^{3+} destabilize the low-temperature lanthanite and end-member hydroxylbastnäsite structures; consequently, Dy-systems culminate in kozoite as the final stable phase. A notable exception occurs in the Dy–aragonite system, where the hydrated phase tengerite [$Dy_2(CO_3)_3{\cdot}2$-$3H_2O$] precipitates as an intermediate phase before transforming to kozoite, highlighting the additional influence of the host mineral's chemistry and dissolution kinetics.[36,37]

The kinetics of replacement are strongly influenced by temperature and the chemistry and structure of the host mineral. While at ambient conditions, the process remains incomplete even over months, even mild hydrothermal conditions (*e.g.*, >80 °C) can drastically accelerate the reactions, enabling complete replacement within days. The host mineral's solubility and dissolution rate are critical; aragonite ($\log K_{sp}$ = −8.34),[39] being more soluble than calcite or dolomite, also has a higher dissolution rate,[40] leading to higher initial supersaturation and faster nucleation of REE phases compared to dolomite ($\log K_{sp}$ = −18.14) and calcite ($\log K_{sp}$ = −8.48). This difference in kinetics can also influence the morphology of the secondary products, often resulting in finer-grained or spherulitic textures on aragonite.

The reaction pathways and final mineral assemblages can become significantly more complex in systems involving multi-component REE solutions, as the ionic radii, concentrations, and individual chemical behaviors of each REE compete during crystallization.[38] Experiments using solutions with equal concentrations of La, Ce, Pr, Nd, and Dy resulted in the formation of relatively homogeneous (La, Ce,

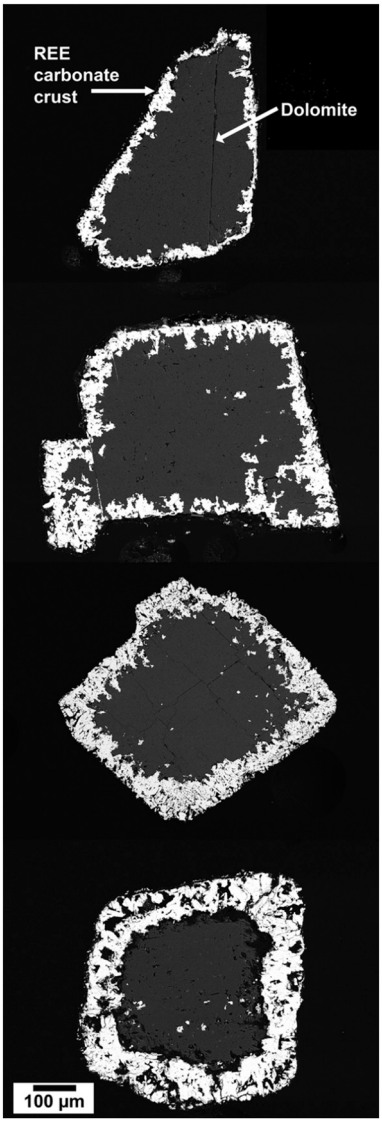

Fig. 6 SEM images showing the progressive replacement of dolomite grains in polished sample pucks. The sequence highlights the advance of the reaction interface and the formation of secondary REE-carbonate phases that progressively consume the original dolomite crystals.

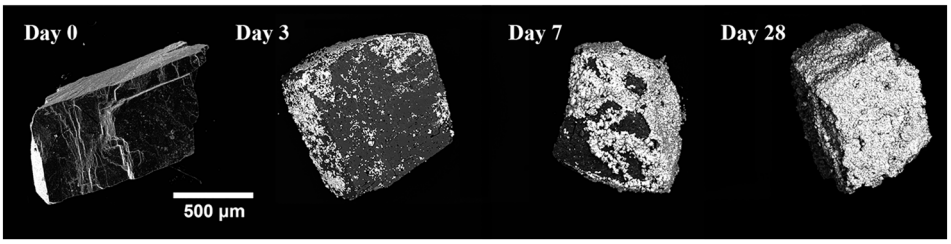

Fig. 5 SEM images illustrating the initial stages of dolomite single-crystal replacement by REE carbonates. A thin surface precipitate layer first develops on dolomite and progressively thickens until the grain is completely covered by the newly formed REE-carbonate phase.

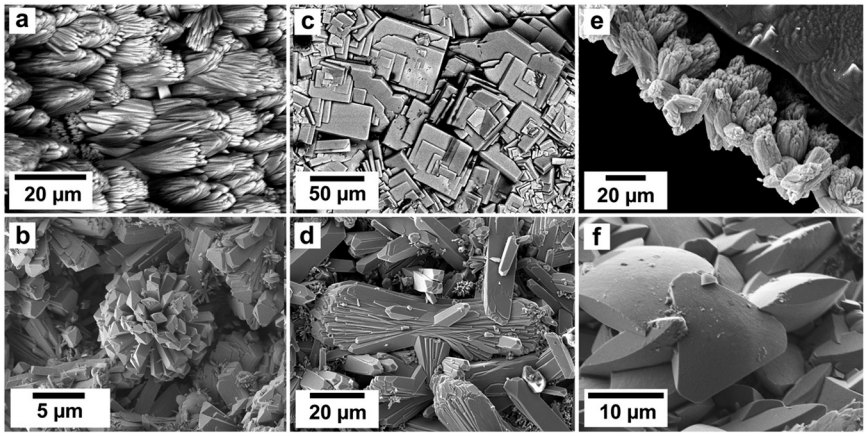

Fig. 7 Different REE-bearing carbonates growing on the surfaces of Ca–Mg carbonates during the solution-mediated replacement reactions: (a) Nd-kozoite replacing dolomite at 165 °C; (b) spherulitic La-kozoite on dolomite at 80 °C; (c) of La-lanthanite replacing aragonite at 21 °C: (d) Ce-kozoite replacing dolomite grains at 50 °C; (e) Dy-kozoite on calcite at 220 °C; (f) La-hydroxylbastnasite on dolomite at 220 °C.

Pr, Nd, Dy)-kozoite solid solutions, with the REE ratios in the solid phase mirroring those in the aqueous solution.[38] In contrast, experiments utilizing solutions with REE concentrations normalized to a Post-Archean Australian Shale (PAAS) standard, which is Ce-dominated, revealed a pronounced partitioning of REEs during replacement. This process resulted in chemically zoned crystals (Fig. 8) and the discrete crystallization of Ce-rich phases (Fig. 9 and 10). In PAAS systems, lighter REEs (La, Ce) were preferentially incorporated into the early overgrowths (Fig. 8), forming crystal cores, while heavier REEs (Nd, Dy) became concentrated in the rims, producing concentric zoning within individual crystals and across the replacement corona. This fractionation reflects kinetic controls: the lower ionic potential of the light REE^{3+} ions promotes faster dehydration and incorporation relative to the heavier REE^{3+} ions. Although lighter REE carbonates are generally considered more soluble than their heavier analogues,[41] the literature reports conflicting trends.[42,43] Such discrepancies likely reflect the complexity of crystallization pathways, where different transient or nanoscale polymorphs, each with

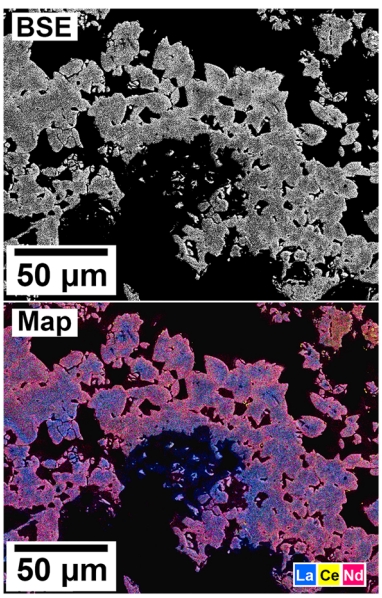

Fig. 8 SEM-BSE image and corresponding EDS elemental map of an aragonite grain reacted at 165 °C for 72 h in PAAS solution. The maps reveal compositional zoning within a kozoite crystal, with lighter rare earth elements concentrated in the core and heavier rare earth elements enriched along the outer margins.

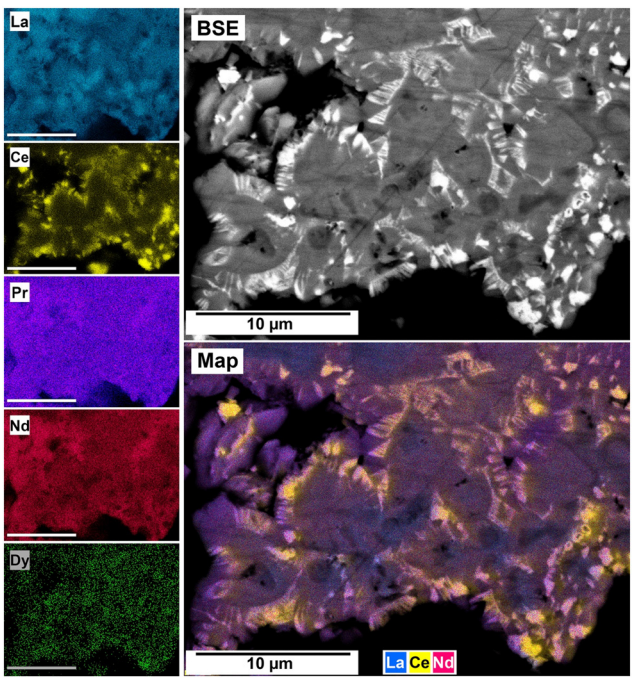

Fig. 9 SEM-BSE image and corresponding EDS elemental map of an aragonite grain reacted at 210 °C for 24 h in PAAS solution. The mapped area reveals a secondary replacement of REE-carbonate phases by cerianite, resulting in symplectic textures that overprint the earlier replacement of aragonite by REE carbonates. The distribution of cerianite delineates the boundaries between pre-existing spindle-shaped kozoite crystals, suggesting preferential nucleation and growth along crystal interfaces during late-stage mineralization.

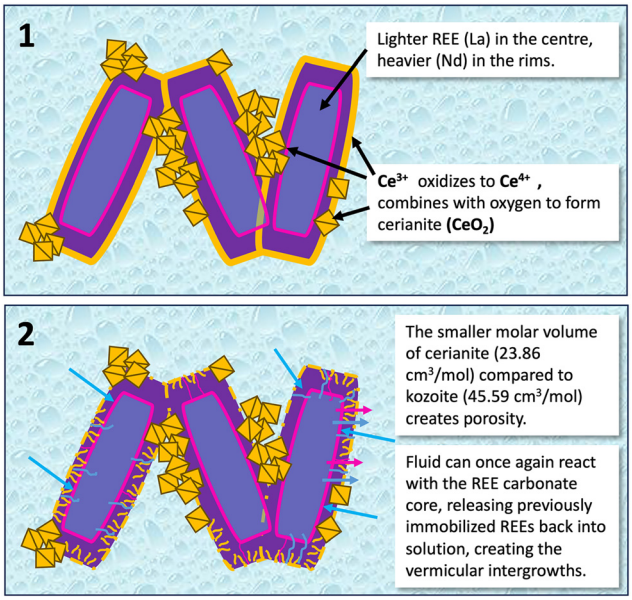

Fig. 10 Schematic diagram depicting the proposed mechanism for the development of symplectic textures during the interaction of Ce-bearing REE fluids with Ca–Mg carbonate minerals. The diagram summarizes the sequence of mineral replacement and phase evolution inferred from experimental observations.

distinct solubility products and growth kinetics, influence observed solubility behavior.

A key concept governing the efficiency and completeness of dissolution–reprecipitation reactions is partial equilibrium.[44–46] This state arises when a newly precipitated REE-rich phase (*e.g.*, kozoite or lanthanite) forms a coherent, impermeable crust on the surface of the dissolving host Ca–Mg carbonate.[36–38,47] The crust acts as a physical barrier, isolating the reactive parent mineral from the bulk solution and thereby halting the reaction before full replacement is achieved. The driving force for this armoring effect is often a pronounced positive molar volume change; for example, the molar volume of REE-carbonates such as lanthanite (≈220.32 $cm^3\ mol^{-1}$)[48] is significantly larger than that of the replaced calcite (≈36.93 $cm^3\ mol^{-1}$).[48] Precipitation directly at the fluid–mineral interface can thus rapidly generate a passivating layer that seals the surface. From this framework, two contrasting scenarios can emerge:

(i) Full replacement despite kinetic slowing: experimental evidence[49] shows that complete replacement of Ca–Mg carbonates can occur, even when intermediate REE-carbonates possess large molar volumes. In these cases, rapid, defect-rich crystallization *via* spherulitic growth produces a porous reaction rim rather than a dense barrier. Although porosity slows down transport, it preserves fluid pathways to the reaction front, thereby enabling full replacement.

(ii) Halted replacement due to epitaxial overgrowths (Fig. 11): when the overgrowth phase shares close structural compatibility with the host (*d*-spacing mismatch typically <10%),[50,51] epitaxial relationships minimize interfacial

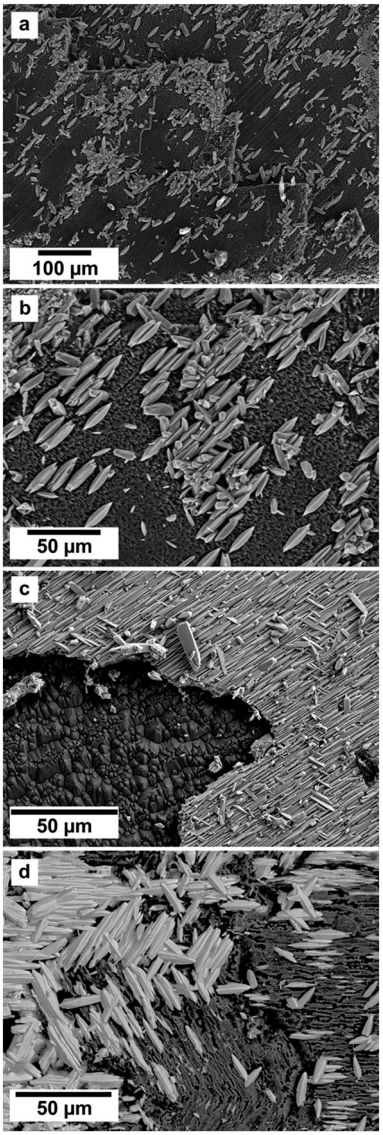

Fig. 11 SEM images showing the epitaxial overgrowths of kozoite on (a and b) calcite and (c and d) aragonite single crystals. On calcite, kozoite nucleates and grows with a single, well-defined crystallographic orientation. In contrast, epitaxial growth on aragonite can occur in three distinct crystallographic orientations.

energy and promote coherent growth along specific crystallographic directions.[45,46] Such epitaxial encapsulation preserves the host core and inhibits further reaction. Importantly, epitaxial control can be transient: oriented overgrowths are often metastable and may later transform into more stable, randomly oriented phases. Examples include metastable kozoite ($REECO_3OH$) epitaxies on calcite,[36] dolomite, or pseudohexagonally twinned aragonite.[47] Upon transformation into hydroxylbastnäsite or cerianite, epitaxial coherence is lost, porosity develops, and the reaction front advances, its extent governed by the relative molar volumes of the phases involved.

Thus, the persistence of partial equilibrium depends on the interplay between structural compatibility, which favors

epitaxial stabilization, and chemical driving forces, which favor transformation. The breakdown of epitaxial coherence marks a critical shift from interface-controlled growth toward transport- or supersaturation-controlled growth, allowing the system to progress toward full thermodynamic equilibrium.[47] In natural settings, the preservation of epitaxial textures provides a diagnostic record of specific physicochemical conditions, such as moderate temperatures and evolving fluid compositions, that modulate dissolution kinetics and reprecipitation pathways.

3.2. Redox-driven replacement reactions: the role or Ce

In both single- and multi-REE systems, the starting pH of the aqueous solution prior to the beginning of the dissolution of the host Ca–Mg carbonates is ≈5.1. Once the host starts dissolving and being replaced by REE carbonates, the pH of the aqueous solution increases towards a value of ≈8.0–8.2 at near-equilibrium conditions. At this higher pH, Ce^{3+} ions become increasingly hydrolyzed, forming Ce–hydroxo complexes. These are more easily oxidized, and under hydrothermal conditions Ce^{3+} is oxidized to Ce^{4+}, as the latter achieves a stable, noble-gas-like electron configuration ($[Xe]4f^0$).[52–54] This process, which is kinetically favored by temperature, has two critical consequences: first is the nucleation and growth of a dense and insoluble (K_{sp} = −59.3)[55] oxide, cerianite ($Ce^{4+}O_2$),[49] due to the inability of Ce^{4+} to form carbonate solids. This oxidation is intrinsically coupled with decarbonation (*e.g.*, $CeCO_3OH_{(s)} \rightarrow CeO_{2(s)} + CO_{2(g)} + H^+_{(aq)} + e^-$), in which CO_2 gas and H^+ ions are released, causing a drastic local acidification of the aqueous solution, promoting further dissolution of any carbonate phases and thus sustaining the reaction front. The oxidation of Ce^{3+} produces crystalline CeO_2 nanoparticles, which act as transient, highly reactive intermediates during carbonate replacement.[49,55,56] Subsequent aggregation and coarsening of these nanoparticles leads to polycrystalline cerianite and the development of porous replacement textures. The large difference between the molar volume of the REE carbonates (*e.g.*, 44.76 $cm^3\ mol^{-1}$ for kozoite; 44.02 $cm^3\ mol^{-1}$ for bastnäsite)[48] compared to cerianite (23.86 $cm^3\ mol^{-1}$)[48] results in an increase in porosity, increasing the reactive surface area, which can accelerate subsequent alteration processes. This way, in hydrothermal conditions (*e.g.*, ≥165 °C), the crystallisation of cerianite leads to the dissolution of pre-existing REE carbonates (kozoite, bastnäsite) until the Ce^{3+} oxidation to Ce^{4+} is completed.

The interaction of host Ca–Mg carbonates with Ce-bearing REE is frequently translated into double-replacement reactions. The initial step involves the replacement of the host by metastable Ce^{3+}-bearing REE carbonate phases (*e.g.*, lanthanite, kozoite, bastnasite). Then, the solution-mediated oxidation of Ce^{3+} to Ce^{4+} results into a new replacement reaction, where the Ce^{3+}-carbonate undergoes *in situ* decarbonation and oxidation to form the final, stable cerianite phase.[38,49] The crystallization of cerianite is a critical sink for Ce and can also incorporate other REEs with similar ionic radii, such as Dy^{3+}, as impurities.[38] However, the extent and completeness of this entire reaction pathway is dependent on the fluid's initial chemistry and temperature. While the initial REE/(Ca + Mg) ratio controls the saturation state and kinetics of the first replacement reaction of the host Ca–Mg carbonate by REE carbonates, the Ce/REE ratio dictates the extent of the secondary replacement. A high Ce/REE ratio promotes the complete dissolution of the Ca–Mg–REE carbonates and the crystallisation of cerianite, creating highly porous pseudomorphs, with the concomitant liberation of non-Ce REEs back to the aqueous solution. A lower Ce/REE ratio may result in the partial preservation of trivalent REE- and/or Ca–Mg-carbonate phases.

The partial replacement of REE carbonates by cerianite generates intricate symplectic textures (Fig. 9 and 10), observed as fine-scale, vermicular intergrowths of Ce^{4+}-rich oxides within a matrix of other REE carbonates. These textures are common in metamorphic rocks that have experienced high PT conditions[57] and have been also observed in REE-bearing deposits.[58] In our experimental system, these are a direct consequence of the large differences in molar volume and solubility between the parent and product phases. The dissolution of kozoite/bastnäsite (molar volume ≈ 45–47 $cm^3\ mol^{-1}$)[48] and precipitation of denser cerianite (molar volume ≈ 23.86 $cm^3\ mol^{-1}$)[48] creates significant porosity (Fig. 10). This porosity allows the reactive fluid to infiltrate further, initiating replacement at the boundaries between pre-existing carbonate crystals. This process is fluid-mediated, driven by interfacial dissolution–precipitation, where Ce^{4+} from the solution reacts with the carbonate, releasing CO_2 and other REE^{3+} back into the fluid. The resulting texture often preserves a "ghost" of the original kozoite/bastnasite crystal morphology, defined by the cerianite that nucleates along its margins and fractures.[38] Furthermore, the oxidation of Ce^{3+} already incorporated within the kozoite/bastnäsite structure can lead to a solid-state exsolution process, where the smaller Ce^{4+} ion becomes incompatible with the carbonate lattice, migrating to form nanoscale cerianite nuclei. These symplectites represent a dynamic, open-system process of element remobilization and re-concentration at the micro- and nanoscale, highlighting that high-grade REE mineralization may involve multiple episodes of dissolution and reprecipitation even after the initial carbonate ore has formed.

Among the REEs, Eu is also redox-active, but its redox behavior differs fundamentally from that of Ce. Reduction of Eu^{3+} to Eu^{2+} requires strongly reducing conditions and does not lead to the formation of an insoluble Eu(II) oxide under hydrothermal conditions. Instead, Eu^{2+} behaves chemically similarly to Ca^{2+} or Sr^{2+}, resulting in enhanced mobility and a strong tendency for lattice substitution rather than discrete mineral precipitation. At low concentrations, Eu^{2+} would be incorporated into carbonate lattices.[32,34] Under specific replacement conditions, however, Eu^{2+} may form a carbonate

phase with an aragonite-type structure.[59] In contrast to the oxidation of Ce^{3+} to Ce^{4+}, which produces insoluble CeO_2 and drives decarbonation and replacement reactions, Eu reduction would promote solid-solution formation, not generating a comparable mineralogical sink.

3.3. Double oxidation and transient REE-carbonate replacement processes

In some hydrothermal environments, coupled oxidation reactions can destabilize thermodynamically stable REE-carbonates, meaning that even phases considered thermodynamically stable, like bastnäsite, may appear only transiently before being dissolved or replaced. Maddin *et al.* (2024)[60] investigated the hydrothermal interaction of siderite ($FeCO_3$) with multi-component REE-bearing fluids (La, Ce, Pr, Nd, Dy), highlighting the critical role of redox reactions in controlling the mineral replacement pathway. The experiments revealed that oxidation of Fe^{2+} to Fe^{3+} (triggering goethite/hematite formation) and Ce^{3+} to Ce^{4+} (resulting in cerianite formation) both release protons into solution. This progressive acidification lowers carbonate stability, triggering decarbonation reactions. As a result, REE carbonates (kozoite, bastnäsite) that may crystallize initially (Fig. 12 and 13) are subsequently dissolved. Ultimately, hematite and cerianite remain as the stable end products, while REEs are either remobilized or trapped in oxides.

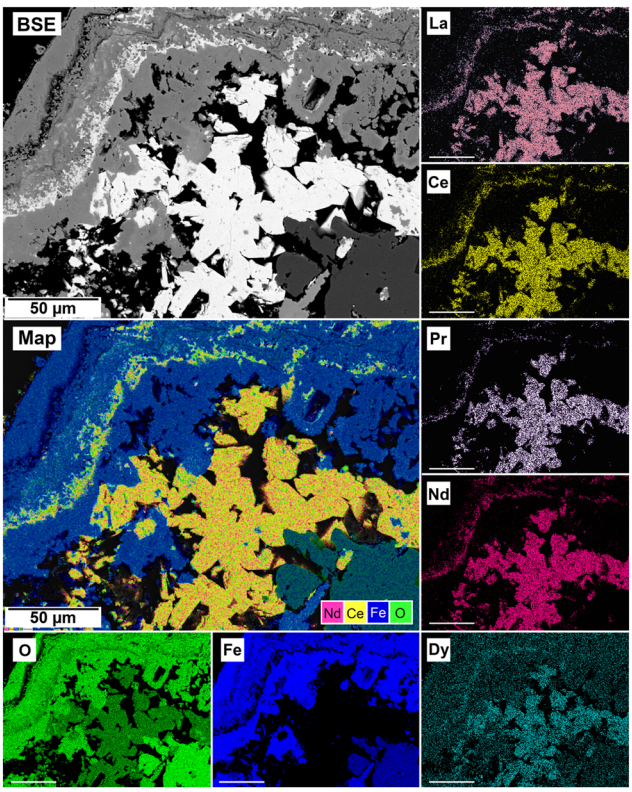

Fig. 12 SEM images and EDS elemental map showing the transient replacement of the siderite host by kozoite in equal-concentration experiments conducted at 165 °C for 24 h.

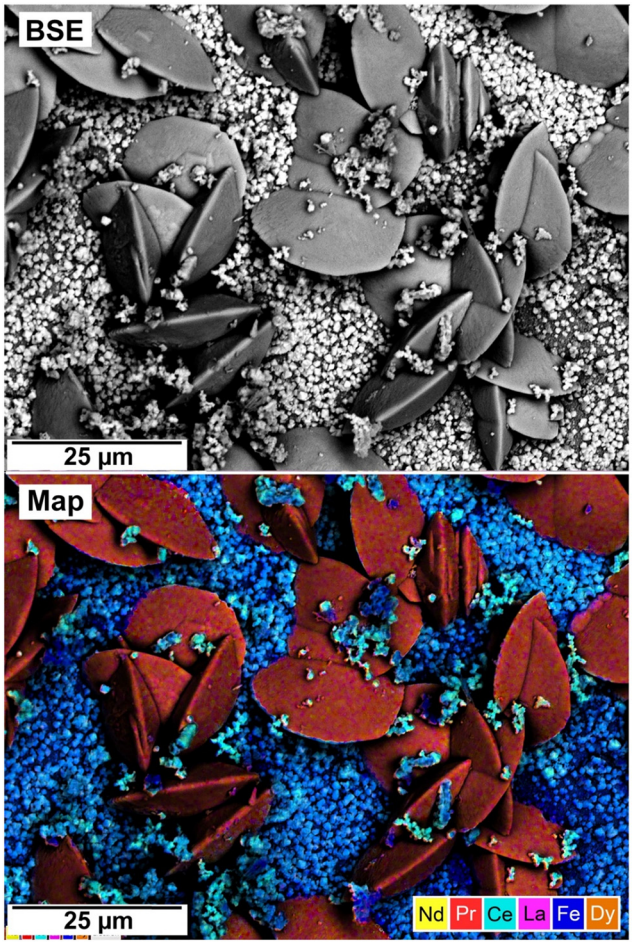

Fig. 13 SEM-BSE image of a siderite grain undergoing replacement by bastnäsite in equal-concentration experiments at 205 °C for 24 h. EDS elemental map reveals an almost homogeneous distribution of REEs, indicating uniform incorporation during the replacement process. The matrix consists of nm-sized grains of cerianite and hematite.

This transient stabilization of REE-carbonates is highly sensitive to both redox conditions and REE availability (Fig. 14). While at lower temperatures, a passivating goethite layer can suppress carbonate replacement, creating a partial equilibrium state, at hydrothermal conditions, dissolution accelerates, allowing for kozoite and bastnäsite crystallization before they are destabilized by ongoing Fe and Ce oxidation. The molar volume contrast between cerianite and the REE-carbonates further enhances replacement, as cerianite's smaller volume facilitates pore formation and continuous fluid access. Ultimately, the interplay between Fe and Ce redox transformations not only governs the pace of carbonate breakdown but also dictates whether REEs in hydrothermal fluids are transiently sequestered in carbonate phases or locked in oxides.

These findings highlight the importance of coupled redox reactions in natural systems where REE-rich fluids interact with Fe^{2+}-bearing carbonates, such as carbonatite-associated ore deposits.[61] The transient crystallization and subsequent dissolution of REE-carbonates under

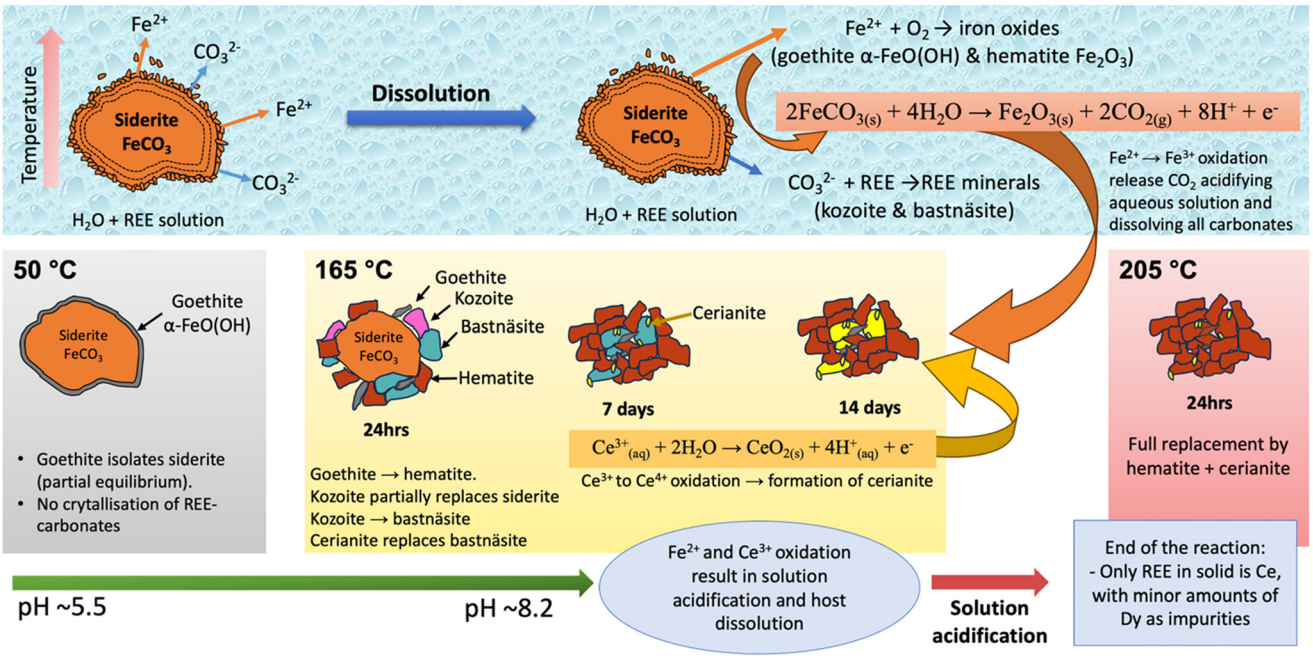

Fig. 14 Schematic diagram depicting the proposed replacement mechanisms during the REE-bearing fluid interaction with siderite. The diagram summarizes the sequence of mineral replacement and phase evolution inferred from experiments conducted at 50, 165, and 205 °C, highlighting temperature-dependent reaction pathways and secondary phase formation.

oxidating conditions help explain the coexistence of metastable REE phases with hematite–cerianite assemblages in natural hydrothermal environments, providing mechanistic insights into both REE mobility and ore formation processes.

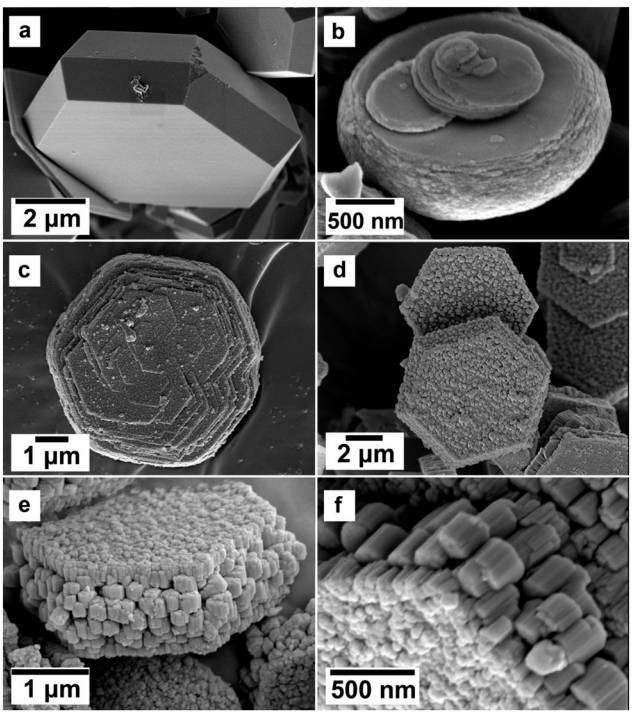

Fig. 15 SEM images illustrating the morphologies of (a) of La- and (b) Nd-fluocerite crystals formed after fluorite (CaF_2); (c and d) progressive replacement of the fluocerite surfaces by REE-carbonates; (e and f) subsequent replacement of fluocerite into Nd-bastnasite at 200 °C forming pseudomorphic crystalline nanoaggregates.

3.4. Fluorine-controlled pathways to bastnasite

Experimental research has demonstrated that in Ca–Mg–REE–CO_3–F systems, fluocerite ($REEF_3$) can also act as a key transient precursor in the hydrothermal formation of REE fluorocarbonates like bastnaesite.[62] Fluocerite forms during the reaction of fluorite with La-, Ce-, and Nd-bearing solutions usually at hydrothermal conditions but even at near-ambient temperatures (*e.g.*, 30–90 °C). Subsequently, in carbonate-bearing solutions, this mineral transforms into bastnäsite (Fig. 15). The kinetics of fluocerite formation is strongly affected by the REE^{3+} ionic radius, with lighter REEs (La) crystallising rapidly, while heavier REEs (Nd) exhibit sluggish nucleation at low temperatures. Activation energies for nucleation ($E_a \approx 81$–96 kJ mol^{-1}) and crystallisation ($E_a \approx 72$–90 kJ mol^{-1}) reveal that REE ionic potential exerts strong control on precursor stability and crystal morphology, ranging from small, rounded fluocerite crystals in La systems to more euhedral hexagonal prisms for Nd (Fig. 15).

Upon carbonation, fluocerite undergoes solution-mediated pseudomorphic replacement, producing bastnäsite as the dominant product, often accompanied by kozoite in Nd systems or cerianite in Ce systems.[62] The transformation initiates through nanocrystalline crusts (~50 nm thickness) on fluocerite surfaces (Fig. 15), which coarsen with time and temperature. Structural similarities between fluocerite and bastnäsite (hexagonal/trigonal symmetry, lattice misfits <

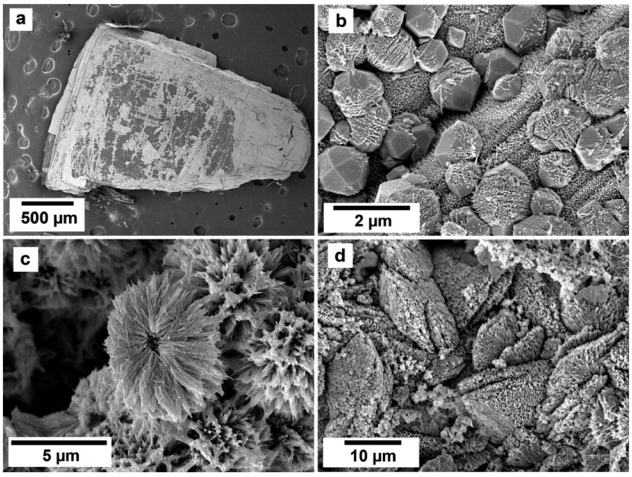

Fig. 16 SEM photomicrographs showing the nanocrystalline solids obtained in experiments during the interaction of vivianite crystals with REE-bearing aqueous solutions. (a) Initial replacement of vivianite by newly formed crystals; (b) growth of giniite crystals on the surface of the vivianite and early stages of growth of rhabdophane on the surface of giniite; (c) rhabdophane spherulitic nanoaggregates covering the surface of the host crystals; (d) monazite and rhabdophane aggregates.

1.5%) promote epitaxial overgrowth, lowering interfacial energy and stabilising the newly nucleated phase. In Ce-bearing systems, temperature-dependent double-replacement reactions are possible (*i.e.*, fluorite → fluocerite → Ce-bastnasite → cerianite), with cubic cerianite (111) planes also growing epitactically on fluocerite (001) surface despite moderate misfits (~8%). The reaction pathway is further governed by thermodynamic and structural constraints: bastnäsite possesses larger molar volume (42.52 $cm^3\ mol^{-1}$)[48] than fluocerite (32.99 $cm^3\ mol^{-1}$),[48] leading to partial isolation of the precursor by product rims and retarding reaction front progression. In contrast, the Ce^{3+} → Ce^{4+} oxidation that produces cerianite reduces molar volume and induces porosity, creating skeletal crystal textures and enhancing fluid access.

Collectively, these findings highlight fluorine as a mechanistic driver of REE mineralisation, lowering REE^{3+} desolvation energies and enabling bastnäsite nucleation under mild hydrothermal conditions (<100 °C). Fluocerite emerges as an essential intermediate phase,[63] capturing REEs from solution and transferring them into stable carbonate or oxide hosts *via* epitaxially controlled growth, sometimes combined with redox transformations (in the case of Ce). This framework explains the presence of some fluocerite remains in natural carbonatite deposits,[10,64–66] refines models of REE ore genesis, and informs strategies for REE recovery and material design.

3.5. Redox-controlled mineral replacement of Fe phosphates

Maddin *et al.* (2025)[67] demonstrated that the replacement of vivianite ($Fe^{2+}{}_3(PO_4)_2{\cdot}8H_2O$) by REE phosphates is strictly dependent on solution-mediated oxidation processes. Under reducing conditions, vivianite is highly insoluble and more stable than REE phosphates such as rhabdophane, $REE(PO_4){\cdot}0.6H_2O$ and monazite, $REEPO_4$, so replacement cannot occur. When Fe^{2+} is oxidized to Fe^{3+}, vivianite is destabilized, dissolved, and phosphate is released into solution, thereby creating the conditions required for REE phosphate precipitation at the fluid–mineral interface (Fig. 16). Without this solution-mediated oxidative step, the dissolution–recrystallisation pathway is both kinetically and thermodynamically inhibited, making oxidation the essential driver of the transformation.[67]

Once initiated, the replacement proceeds pseudomorphically: vivianite is progressively consumed and substituted by REE phosphates (Fig. 16 and 17). Rhabdophane typically forms first,[68] later transforming into monazite as the system evolves toward thermodynamic stability. The process is accompanied by precipitation of Fe^{3+} phosphates and oxides in the surrounding medium, a clear indicator of its redox-driven nature. By linking vivianite destabilization to Fe oxidation, Maddin *et al.* (2025)[67] (Fig. 17), provide a mechanistic explanation for how REE phosphates form in natural environments where fluctuating redox states both mobilize Fe and enhance REE availability. These results clarify the geochemical controls on phosphate-hosted REE mineralizations and emphasize that redox gradients can determine whether REEs are sequestered into stable phosphate phases or remain mobile in solution.

4. Turning waste into REE-source: eggshells as sustainable sorbents for REE recovery

The recovery of REEs increasingly relies on sorbent materials that are both effective and environmentally benign. Biogenic and waste-derived sorbents such as coal fly ash and its derivatives, clay and nanoclay materials (*e.g.*, bentonite), biochar, diatomite and other carbonate hosts have shown significant promise for metal recovery and water decontamination in recent studies, with ongoing work examining synthesis, modification strategies, and mechanisms of uptake and regeneration (*e.g.*, biowaste-derived green sorbents; fly ash as trace metal adsorbent; municipal waste fly ash-derived zeolites; clay nanomaterials; broader assessments of carbon- and inorganic-based sorbents).[69–74] For example, REEs can be extracted from coal fly ash using mild biodegradable acids and subsequently precipitated as oxalates, demonstrating how industrial waste can be valorized within a green chemistry framework.[75] Similar approaches using natural sorbents emphasize ion exchange and dissolution–precipitation mechanisms that avoid reliance on aggressive mineral acids,[76] while opening pathways for sustainable REE capture from aqueous solutions.

Within this context, eggshells have emerged as a versatile, low-cost sorbent. Composed primarily of biogenic calcite with

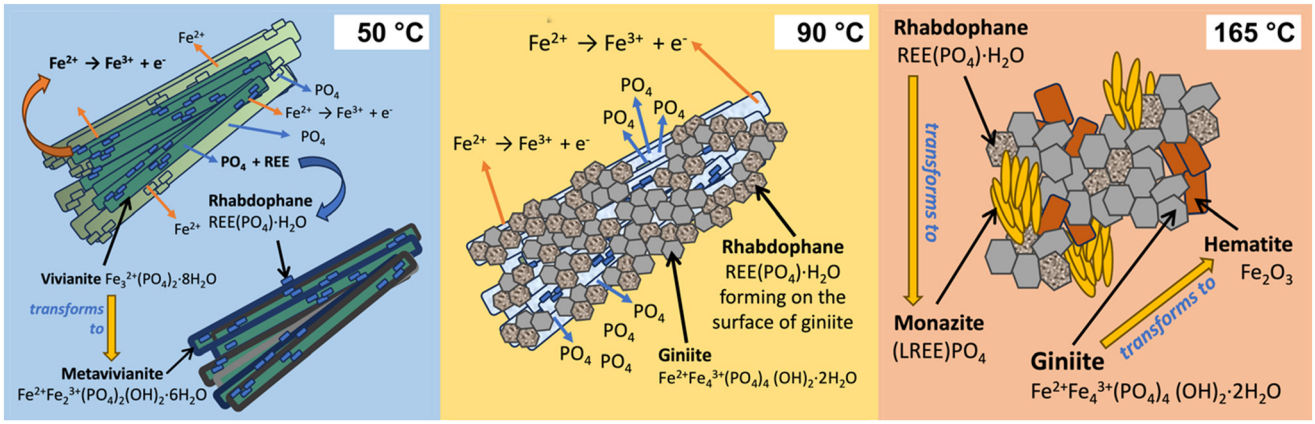

Fig. 17 Schematic diagram depicting the proposed replacement mechanisms during the REE-bearing fluid interaction with vivianite. The diagram summarizes the sequence of mineral replacement and phase evolution inferred from experiments conducted at 50, 90, and 165 °C, highlighting temperature-dependent reaction pathways and secondary phase formation.

a minor organic fraction, eggshells are produced in enormous quantities as food industry waste (~10 Mt annually).[77] They have been investigated to capture light REEs such as La and Ce at moderate pH,[78–80] situating them as a promising sorbent for both environmental remediation and critical metal recovery.

Building on this foundation, Rateau *et al.* (2024)[81] provided a systematic investigation of REE uptake by eggshell calcite under controlled hydrothermal conditions. By exposing eggshell calcite to mixed REE solutions (La, Nd, Dy) across a temperature range from ambient (~25 °C) to 205 °C over periods of up to three months, they demonstrated that the dominant uptake mechanism shifts with temperature. At low temperatures (<90 °C), REEs were incorporated slowly *via* diffusion pathways associated with intracrystalline organics and crystal-boundary networks (Fig. 18). At ~90 °C, surface precipitation of kozoite was observed as spherulitic overgrowths on dissolving calcite surfaces. Above ~165 °C, interface-coupled dissolution–precipitation dominated, with pseudomorphic replacement of calcite by polycrystalline REE carbonates, progressing from kozoite toward hydroxylbastnäsite at the highest temperatures. Mineralogical and microstructural analyses revealed that partitioning among La, Nd, and Dy varied with mechanism and thermal regime, underscoring the complexity of REE distribution in dynamic sorbent systems.

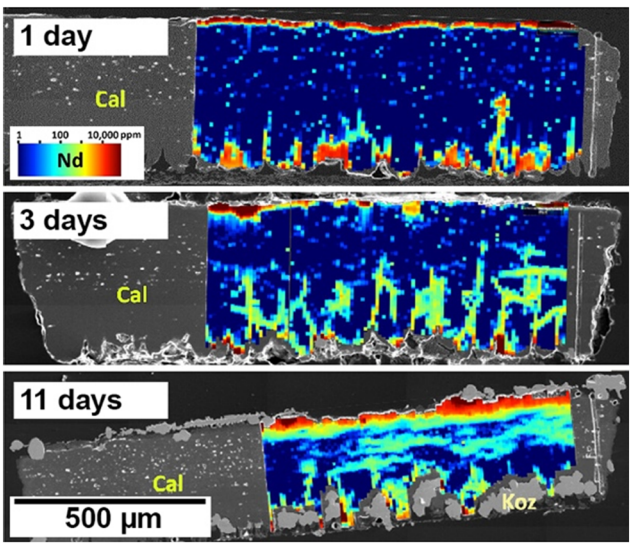

Fig. 18 Laser ablation inductively coupled plasma mass spectrometry analyses illustrating the concentration and spatial distribution of Nd in eggshell calcite after reaction at 90 °C for (a) 1 day, (b) 3 days, and (c) 11 days. The maps reveal progressive Nd incorporation and redistribution within the calcite-bearing shell over time.

From an application perspective, these results identify two potential operational regimes. At lower temperatures, eggshells act primarily as adsorbents/absorbents, favoring diffusion and surface binding under mild conditions where energy inputs are limited. At elevated temperatures, they function as sacrificial templates for REE carbonate precipitation, allowing both capture and conversion into stable solid forms. Rateau *et al.* (2024)[81] show that understanding the kinetics and pathways of REE carbonate formation enables more efficient and selective recovery using eggshell calcite. Eggshell calcite is not intended to compete with engineered sorbents or downstream separation technologies such as flotation or solvent extraction. Instead, it provides a chemically simple, waste-derived carbonate system that allows mechanistic investigation of REE uptake across adsorption, surface precipitation, and mineral replacement regimes. Hydrothermal conditions were employed to accelerate these processes and delineate their kinetic and mineralogical controls; similar mechanisms may operate at lower temperatures over longer timescales or in geothermal and leaching environments. More broadly, their study highlights the potential of waste-to-resource approaches in green chemistry, while emphasizing the necessity of detailed mechanistic understanding to translate laboratory findings into scalable, sustainable technologies.

5. Concluding remarks

Rare-earth element mineralisation as carbonates and phosphates is governed by a combination of processes, including crystallisation from solution and replacement reactions within carbonate hosts. Both general pathways are strongly influenced by fluid chemistry, temperature, redox state, and mineral reactivity, and together they explain the complex mineralogical assemblages, textures, and chemical zoning that characterise many natural REE deposits. Crystallisation from solution highlights the role of amorphous precursors and metastable intermediates in governing phase stability, growth rates, and crystal morphologies, while replacement underscores the capacity of hydrothermal fluids to dissolve, reprecipitate, and trap REEs into more stable carbonate, phosphate and oxide phases.

The study of REE carbonate and phosphate crystallization from solution has emerged as a critical intersection of geology, industrial metallurgy, and materials science. Understanding how REE carbonates crystallise from amorphous precursors, through metastable phases to stable bastnäsite or monazite helps explain natural ore formation and provides a basis for improving the efficiency and selectivity of industrial extraction. Such control is vital given the classification REE as critical elements due to their indispensable roles in permanent magnets, lasers, catalysts, pollution control, and clean energy technologies. A persistent bottleneck has been the lack of detailed knowledge on the earliest stages of crystallization, but recent advances now demonstrate how temperature, ionic radius and ionic potential strongly dictate both phase stability and transformation kinetics. Beyond ore processing, the ability to steer crystallization pathways offers opportunities for sustainable recycling from secondary sources and the selective recovery of REEs from dilute streams. Furthermore, tailoring REE mineral size, shape and morphology is a key design feature for creating high-surface-area catalytic or functional materials in synthetic systems and opens avenues for designing solids with specific optical, catalytic, or magnetic properties. In sum, the capacity to control REE crystallization represents both a scientific challenge and a technological opportunity, central to securing future supply chains and expanding applications of these critical elements.

Author contributions

Juan Diego Rodriguez-Blanco: conceptualization, funding acquisition, resources, investigation, methodology, project administration, supervision, validation, visualization, writing – original draft. Melanie Maddin: formal analysis, data curation, investigation, validation, visualization. Remi Rateau: formal analysis, investigation, data curation, validation, visualization. Adrienn Maria Szucs: formal analysis, investigation, data curation, validation, visualization. Luca Terribili: formal analysis, investigation, validation, data curation, visualization. Beatriz Vallina: formal analysis, investigation, validation, data curation, visualization. Kristina Petra Zubovic: formal analysis, investigation.

Conflicts of interest

There are no conflicts to declare.

Data availability

No primary research results, software or code have been included and no new data were generated or analysed as part of this review.

Acknowledgements

Remi Rateau, Melanie Maddin, Luca Terribili, Kristina Petra Zubovic, and Juan Diego Rodriguez-Blanco acknowledge that this publication is based on research supported in part by Science Foundation Ireland (now Research Ireland), the Geological Survey of Ireland, and the Environmental Protection Agency under the SFI Frontiers for the Future Programme (19/FFP/6771; project no. 210281, award no. 16370). Adrienn Maria Szucs acknowledges a Trinity College Dublin Provost PhD Award, generously funded through alumni donations and Trinity's Commercial Revenue Unit. Beatriz Vallina acknowledges the supported by the Marie Curie EU-FP7 CO2-REACT Research and Training Network under contract RG.EVE.10.1025-004 and the Spanish Ministry of Science and Innovation (MICINN-12-MAT2011-27573-C04-02).

References

1 V. Balaram, Rare earth elements: A review of applications, occurrence, exploration, analysis, recycling, and environmental impact, *Geosci. Front.*, 2019, **10**, 1285–1303.
2 G. Haxel, *Rare earth elements: critical resources for high technology*, US Department of the Interior, US Geological Survey, 2002, vol. 87, no. 2.
3 B. Zhou, Z. Li and C. Chen, Global potential of rare earth resources and rare earth demand from clean technologies, *Minerals*, 2017, **7**, 203.
4 Y. Chen and B. Zheng, What happens after the rare earth crisis: A systematic literature review, *Sustainability*, 2019, **11**, 1288.
5 M. Traore, A. Gong, Y. Wang, L. Qiu, Y. Bai, W. Zhao, Y. Liu, Y. Chen, Y. Liu, H. Wu, S. Li and Y. You, Research progress of rare earth separation methods and technologies, *J. Rare Earths*, 2023, **41**, 182–189.
6 F. Wall, Rare earth elements, in *Critical metals handbook, 312–339*, ed. G. Gunn, American Geophysical Union, John Wiley & Sons, Ltd., 2014, p. 454.
7 A. E. Williams-Jones, A. A. Migdisov and I. M. Samson, Hydrothermal mobilisation of the rare earth elements–a tale of "ceria" and "yttria", *Elements*, 2012, **8**, 355–360.
8 A. A. Migdisov and A. E. Williams-Jones, Hydrothermal transport and deposition of the rare earth elements by

fluorine-bearing aqueous liquids, *Miner. Deposita*, 2014, **49**, 987–997.

9 A. Migdisov, X. Guo, H. Nisbet, H. Xu and A. E. Williams-Jones, Fractionation of REE, U, and Th in natural ore-forming hydrothermal systems: Thermodynamic modeling, *J. Chem. Thermodyn.*, 2019, **128**, 305–319.

10 A. C. Strzelecki, A. Migdisov and H. Boukhalfa, Fluocerite as a precursor to rare earth element fractionation in ore-forming systems, *Nat. Geosci.*, 2022, **15**, 327–333.

11 A. Chakrabarty, R. H. Mitchell, M. Ren, A. K. Sen and K. L. Pruseth, Rinkite, cerianite-(Ce), and hingganite-(Ce) in syenite gneisses from the Sushina Hill Complex, India: occurrence, compositional data and petrogenetic significance, *Mineral. Mag.*, 2013, **77**, 3137–3153.

12 S. M. Jowitt, T. T. Werner, Z. Weng and G. M. Mudd, Recycling of the rare earth elements, *Curr. Opin. Green Sustainable Chem.*, 2018, **13**, 1–7.

13 L. Terribili, A. M. Szucs, M. Maddin, K. P. Zubovic, R. Rateau and J. D. Rodriguez-Blanco, Mechanistic Insights into the Early-Stage Crystallization and Nanophase Formation of Metastable Light Rare-Earth Carbonates, *Cryst. Growth Des.*, 2025, **25**, 945–962.

14 B. Vallina, J. D. Rodriguez-Blanco, A. P. Brown, J. A. Blanco and L. G. Benning, Amorphous dysprosium carbonate: characterization, stability, and crystallization pathways, *J. Nanopart. Res.*, 2013, **15**, 1438.

15 B. Vallina, J. D. Rodriguez-Blanco, J. A. Blanco and L. G. Benning, The effect of heating on the morphology of crystalline neodymium hydroxycarbonate, $NdCO_3OH$, *Mineral. Mag.*, 2014, **78**, 1391–1397.

16 B. Vallina, J. D. Rodriguez-Blanco, A. P. Brown, J. A. Blanco and L. G. Benning, The role of amorphous precursors in the crystallization of La and Nd carbonates, *Nanoscale*, 2015, **7**, 12166–12179.

17 J. D. Rodriguez-Blanco, S. Shaw and L. G. Benning, The kinetics and mechanisms of amorphous calcium carbonate (ACC) crystallization to calcite, via vaterite, *Nanoscale*, 2011, **3**, 265–271.

18 P. Bots, L. G. Benning, J. D. Rodriguez-Blanco, T. Roncal-Herrero and S. Shaw, Mechanistic insights into the crystallization of amorphous calcium carbonate (ACC), *Cryst. Growth Des.*, 2012, **12**, 3806–3814.

19 J. D. Rodriguez-Blanco, S. Shaw, P. Bots, T. Roncal-Herrero and L. G. Benning, The role of pH and Mg on the stability and crystallization of amorphous calcium carbonate, *J. Alloys Compd.*, 2012, **536**, S477–S479.

20 J. D. Rodriguez-Blanco, S. Shaw, P. Bots, T. Roncal-Herrero and L. G. Benning, The role of Mg in the crystallization of monohydrocalcite, *Geochim. Cosmochim. Acta*, 2014, **127**, 204–220.

21 J. D. Rodriguez-Blanco, S. Shaw and L. G. Benning, A route for the direct crystallization of dolomite, *Am. Mineral.*, 2015, **100**, 1172–1181.

22 J. D. Rodriguez-Blanco, K. K. Sand and L. G. Benning, ACC and vaterite as intermediates in the solution-based crystallization of $CaCO_3$, in *New Perspectives on Mineral Nucleation and Growth: From Solution Precursors to Solid Materials*, Springer International Publishing, Cham, 2017, pp. 93–111.

23 J. D. Rodriguez-Blanco, B. Vallina, J. A. Blanco and L. G. Benning, The role of REE^{3+} in the crystallization of lanthanites, *Mineral. Mag.*, 2014, **78**, 1373–1380.

24 L. Gránásy, T. Pusztai, G. Tegze, J. A. Warren and J. F. Douglas, Growth and form of spherulites, *Phys. Rev. E*, 2005, **72**, 011605.

25 J. P. Andreassen, E. M. Flaten, R. Beck and A. E. Lewis, Investigations of spherulitic growth in industrial crystallization, *Chem. Eng. Res. Des.*, 2010, **88**, 1163–1168.

26 L. B. Railsback, An earth scientist's periodic table of the elements and their ions, *Geology*, 2003, **31**, 737–740.

27 G. H. Cartledge, Studies on the periodic system. I. the ionic potential as a periodic function, *J. Am. Chem. Soc.*, 1928, **50**, 2855–2863.

28 G. H. Cartledge, Studies on the Periodic System. II. The Ionic Potential and Related Properties, *J. Am. Chem. Soc.*, 1928, **50**, 2863–2872.

29 P. P. Fedorov, M. V. Nazarkin and R. M. Zakalyukin, On polymorphism and morphotropism of rare earth sesquioxides, *Crystallogr. Rep.*, 2002, **47**, 281–286.

30 L. Terribili, R. Rateau, A. M. Szucs, M. Maddin and J. D. Rodriguez-Blanco, Impact of rare earth elements on $CaCO_3$ crystallization: insights into kinetics, mechanisms, and crystal morphology, *Cryst. Growth Des.*, 2024, **24**, 632–645.

31 P. Raiteri and J. D. Gale, Water is the key to nonclassical nucleation of amorphous calcium carbonate, *J. Am. Chem. Soc.*, 2010, **132**, 17623–17634.

32 M. Schmidt, T. Stumpf, M. Marques Fernandes, C. Walther and T. Fanghänel, Charge compensation in solid solutions, *Angew. Chem., Int. Ed.*, 2008, **47**, 5846–5850.

33 Y. Zhang and R. A. Dawe, Influence of Mg^{2+} on the kinetics of calcite precipitation and calcite crystal morphology, *Chem. Geol.*, 2000, **163**, 129–138.

34 M. Schmidt, T. Stumpf, C. Walther, H. Geckeis and T. Fanghänel, Phase transformation in $CaCO_3$ polymorphs: A spectroscopic, microscopic and diffraction study, *J. Colloid Interface Sci.*, 2010, **351**, 50–56.

35 A. P. Jones, F. Wall and C. T. Williams, *Rare earth minerals: chemistry, origin and ore deposits*, Springer Science+Business Media, 1996, vol. 7.

36 A. M. Szucs, A. Stavropoulou, C. O'Donnell, S. Davis and J. D. Rodriguez-Blanco, Reaction pathways toward the formation of bastnäsite: Replacement of calcite by Rare Earth carbonates, *Cryst. Growth Des.*, 2021, **21**, 512–527.

37 A. M. Szucs, M. Maddin, D. Brien, P. C. Guyett and J. D. Rodriguez-Blanco, Targeted Crystallization of Rare Earth Carbonate Polymorphs at Hydrothermal Conditions via Mineral Replacement Reactions, *Global Chall.*, 2023, **7**, 2200085.

38 M. Maddin, R. Rateau, A. M. Szucs, L. Terribili, B. Hoare, P. C. Guyett and J. D. Rodriguez-Blanco, Chemical Textures on Rare Earth Carbonates: An Experimental Approach to

Mimic the Formation of Bastnäsite, *Global Chall.*, 2024, **8**, 2400074.

39 L. N. Plummer and E. Busenberg, The solubilities of calcite, aragonite and vaterite in CO_2-H_2O solutions between 0 and 90 C, and an evaluation of the aqueous model for the system $CaCO_3$-CO_2-H_2O, *Geochim. Cosmochim. Acta*, 1982, **46**, 1011–1040.

40 L. E. I. Chou, R. M. Garrels and R. Wollast, Comparative study of the kinetics and mechanisms of dissolution of carbonate minerals, *Chem. Geol.*, 1989, **78**, 269–282.

41 F. H. Firsching and J. Mohammadzadei, Solubility products of the rare-earth carbonates, *J. Chem. Eng. Data*, 1986, **31**, 40–42.

42 M. Voigt, J. D. Rodriguez-Blanco, B. Vallina, L. G. Benning and E. H. Oelkers, An experimental study of hydroxylbastnasite solubility in aqueous solutions at 25 °C, *Chem. Geol.*, 2016, **430**, 70–77.

43 M. E. Essington and S. V. Mattigod, Lanthanide solid phase speciation, *Soil Sci. Soc. Am. J.*, 1985, **49**, 1387–1393.

44 H. C. Helgeson, Evaluation of irreversible reactions in geochemical processes involving minerals and aqueous solutions—I. Thermodynamic relations, *Geochim. Cosmochim. Acta*, 1968, **32**, 853–877.

45 J. D. Rodríguez-Blanco, A. Jiménez and M. Prieto, Oriented overgrowth of pharmacolite ($CaHAsO_4{\cdot}2H_2O$) on gypsum ($CaSO_4{\cdot}2H_2O$), *Cryst. Growth Des.*, 2007, **7**, 2756–2763.

46 J. D. Rodríguez, A. Jiménez, M. Prieto, L. Torre and S. Garcia-Granda, Interaction of gypsum with As(V)-bearing aqueous solutions: Surface precipitation of guerinite, sainfeldite, and $Ca_2NaH(AsO_4)_2{\cdot}6H_2O$, a synthetic arsenate, *Am. Mineral.*, 2008, **93**, 928–939.

47 A. M. Szucs, R. Rateau, M. Maddin and J. D. Rodriguez-Blanco, Transient Epitaxial Growth of Rare Earth Carbonates during Low-Temperature Replacement of Calcite, Aragonite, and Dolomite, *Cryst. Growth Des.*, 2025, **25**, 9275–9287.

48 A. V. Chichagov, D. A. Varlamov, R. A. Dilanyan, T. N. Dokina, N. A. Drozhzhina, O. L. Samokhvalova and T. V. Ushakovskaya, MINCRYST: A crystallographic database for minerals, local and network (WWW) versions, *Crystallogr. Rep.*, 2001, **46**, 876–879.

49 A. M. Szucs, M. Maddin, D. Brien, R. Rateau and J. D. Rodriguez-Blanco, The role of nanocerianite (CeO_2) in the stability of Ce carbonates at low-hydrothermal conditions, *RSC Adv.*, 2023, **13**, 6919–6935.

50 A. G. Walton, Nucleation of Crystals from Solution: Mechanisms of precipitation are fundamental to analytical and physiological processes, *Science*, 1965, **148**, 601–607.

51 Z. Lin, A. Yin, J. Mao, Y. Xia, N. Kempf, Q. He, Y. Wang, C. Y. Chen, Y. Zhang, V. Ozolins and Z. Ren, Scalable solution-phase epitaxial growth of symmetry-mismatched heterostructures on two-dimensional crystal soft template, *Sci. Adv.*, 2016, **2**, e1600993.

52 B. A. Bilal and E. Müller, Thermodynamic study of Ce^{4+}/Ce^{3+} redox reaction in aqueous solutions at elevated temperatures: 1. Reduction potential and hydrolysis equilibria of Ce^{4+} in $HClO_4$ solutions, *Z. Naturforsch., A: Phys. Sci.*, 1992, **47**, 974–984.

53 L. M. Ernst and V. Puntes, How does immunomodulatory nanoceria work? ROS and immunometabolism, *Front. Immunol.*, 2022, **13**, 750175.

54 D. G. Brookins, *Eh-pH diagrams for geochemistry*, Springer Science Business Media, 2012.

55 T. V. Plakhova, A. Y. Romanchuk, S. N. Yakunin, T. Dumas, S. Demir, S. Wang, S. G. Minasian, D. K. Shuh, T. Tyliszczak, A. A. Shiryaev and A. V. Egorov, Solubility of nanocrystalline cerium dioxide: Experimental data and thermodynamic modeling, *J. Phys. Chem. C*, 2016, **120**, 22615–22626.

56 A. Ikeda-Ohno, C. Hennig, S. Weiss, T. Yaita and G. Bernhard, Hydrolysis of tetravalent cerium for a simple route to nanocrystalline cerium dioxide: an in situ spectroscopic study of nanocrystal evolution, *Chem. – Eur. J.*, 2013, **19**, 7348–7360.

57 T. Wang, J. Zheng, J. M. Scott, X. Ping, Q. Ma, Q. Xiong and S. Zhang, Coronitic and symplectitic textures in meta-troctolite reveal the transition from magmatism to granulite-facies metamorphism in the early Paleozoic Tongbai Orogen, Central China, *J. Petrol.*, 2022, **63**, egac060.

58 M. P. Smith, P. Henderson and Z. Peishan, Reaction relationships in the Bayan Obo Fe-REE-Nb deposit Inner Mongolia, China: implications for the relative stability of rare-earth element phosphates and fluorocarbonates, *Contrib. Mineral. Petrol.*, 1999, **134**, 294–310.

59 I. Mayer, E. Levy and A. Glasner, The Crystal Structure of $EuSO_4$ and $EuCO_3$, *Acta Crystallogr.*, 1964, **17**, 1071–1072.

60 M. Maddin, R. Rateau, A. M. Szucs, L. Terribili and J. D. Rodriguez-Blanco, Transient crystallisation of rare earth carbonates during the hydrothermal oxidation of siderite, *RSC Adv.*, 2024, **14**, 35305–35322.

61 X. W. Huang and G. Beaudoin, Textures and chemical compositions of magnetite from iron oxide copper-gold (IOCG) and Kiruna-type iron oxide-apatite (IOA) deposits and their implications for ore genesis and magnetite classification schemes, *Econ. Geol.*, 2019, **114**, 953–979.

62 L. Terribili, R. Rateau, M. Maddin and J. D. Rodriguez-Blanco, The role of fluocerite in the genesis of bastnäsite: mechanistic insights and transformation pathways, *Nanoscale*, 2024, **16**, 13183–13196.

63 M. M. Müller, H. J. Kleebe, S. Lauterbach and G. Zito, Crystallographic orientation relationship between bastnaesite, fluocerite and cerianite observed in a crystal from the pikes peak pegmatites, *Z. Kristallogr.*, 2011, **226**, 467–475.

64 W. Zhang, W. T. Chen and A. E. Williams-Jones, An unique, fluocerite-rich REE deposit in Henan province, Central China: the missing link in magmatic-hydrothermal REE mineralizing systems?, *Contrib. Mineral. Petrol.*, 2023, **178**, 34.

65 D. Holtstam and U. B. Andersson, The REE minerals of the Bastnas-type deposits, south-central Sweden, *Can. Mineral.*, 2007, **45**, 1073–1114.

66 G. J. Beukes, H. de Bruiyn and W. A. van der Westhuizen, Fluocerite and associated minerals from the Baviaanskranz granite pegmatite near Kakamas, South Africa, *S. Afr. J. Geol.*, 1991, **94**, 313–330.

67 M. Maddin, L. Terribili, R. Rateau, A. M. Szucs and J. D. Rodriguez-Blanco, Nanophase REE phosphate crystallization induced by vivianite oxidation: mechanistic insights and mineralogical implications, *RSC Adv.*, 2025, **15**, 11257–11270.

68 T. Roncal-Herrero, J. D. Rodríguez-Blanco, E. H. Oelkers and L. G. Benning, The direct precipitation of rhabdophane ($REEPO_4{\cdot}nH_2O$) nano-rods from acidic aqueous solutions at 5–100° C, *J. Nanopart. Res.*, 2011, **13**, 4049–4062.

69 S. J. Köhler, P. Cubillas, J. D. Rodríguez-Blanco, C. Bauer and M. Prieto, Removal of cadmium from wastewaters by aragonite shells and the influence of other divalent cations, *Environ. Sci. Technol.*, 2007, **41**, 112–118.

70 S. E. Kuh and D. S. Kim, Removal characteristics of cadmium ion by waste egg shell, *Environ. Technol.*, 2000, **21**, 883–890.

71 J. O. Ighalo, Biowastes and derived green sorbents for water decontamination: Insights on thermochemical conversion strategies, *Curr. Opin. Green Sustainable Chem.*, 2024, **45**, 100880.

72 A. Munyengabe, M. Banda, W. Augustyn, K. Netshiongolwe and D. Ramutshatsha-Makhwedzha, Application of coal fly ash for trace metal adsorption from wastewater: A review, *Heliyon*, 2024, **10**, e31494.

73 N. Sheraz, A. Shah, A. Haleem and F. J. Iftikhar, Comprehensive assessment of carbon-, biomaterial-and inorganic-based adsorbents for the removal of the most hazardous heavy metal ions from wastewater, *RSC Adv.*, 2024, **14**, 11284–11310.

74 M. Molina-Fernández, A. Santos Silva, R. Prado Feitosa, E. C. Silva-Filho, J. A. Osajima, S. Medina-Carrasco and M. D. M. Orta Cuevas, Clay Nanomaterials Sorbents for Cleaner Water: A Sustainable Application for the Mining Industry, *Nanomaterials*, 2025, **15**, 1211.

75 A. K. Sakr, S. Praneeth, M. Dardona, D. K. Porter, C. M. Tummala, P. K. Roy and T. M. Dittrich, Potential for eco-friendly recovery of rare earth elements from fly ash using carboxylic acids: A comparative study with mineral acids and environmental risk assessment for sustainable fly ash reuse, *Chem. Eng. J.*, 2025, **503**, 158355.

76 G. A. Moldoveanu and V. G. Papangelakis, An overview of rare-earth recovery by ion-exchange leaching from ion-adsorption clays of various origins, *Mineral. Mag.*, 2016, **80**, 63–76.

77 J. MacNeil, Method and apparatus for separating a protein membrane and shell material in waste egg shells, *US Pat.*, US09/757988, 2001.

78 F. Granados-Correa and M. Jiménez-Reyes, Kinetic, equilibrium and thermodynamic studies on the adsorption of Eu (III) by eggshell from aqueous solutions, *Adsorpt. Sci. Technol.*, 2013, **31**, 891–902.

79 S. S. Metwally, R. R. Ayoub and H. F. Aly, Utilization of low-cost sorbent for removal and separation of ^{134}Cs, ^{60}Co and $^{152+154}Eu$ radionuclides from aqueous solution, *J. Radioanal. Nucl. Chem.*, 2014, **302**, 441–449.

80 E. Salinas Rodríguez, E. A. Cárdenas-Reyes, F. R. Barrientos-Hernández, J. Flores-Badillo, M. P. Gutiérrez-Amador, A. Sánchez-Castillo, O. A. Acevedo-Sandoval, E. Cerecedo-Sáenz and J. Hernández-Ávila, Ce and Nd Extraction by Cationic Exchange, Using Bentonite, Diatomite, and Eggshell—Preliminary Study, *Minerals*, 2023, **13**, 735.

81 R. Rateau, M. Maddin, A. M. Szucs, L. Terribili, K. Drost, P. C. Guyett and J. D. Rodriguez-Blanco, Utilization of Eggshell Waste Calcite as a Sorbent for Rare Earth Element Recovery, *ACS Omega*, 2024, **9**, 25986–25995.

82 E. Curti, Coprecipitation of radionuclides with calcite: estimation of partition coefficients based on a review of laboratory investigations and geochemical data, *Appl. Geochem.*, 1999, **14**, 433–445.

83 E. J. Elzinga, R. J. Reeder, S. H. Withers, R. E. Peale, R. A. Mason, K. M. Beck and W. P. Hess, EXAFS study of rare-earth element coordination in calcite, *Geochim. Cosmochim. Acta*, 2022, **66**, 2875–2885.

84 S. E. Hellebrandt, S. Hofmann, N. Jordan, A. Barkleit and M. Schmidt, Incorporation of Eu (III) into calcite under recrystallization conditions, *Sci. Rep.*, 2016, **6**, 33137.

85 S. Hofmann, K. Voïtchovsky, M. Schmidt and T. Stumpf, Trace concentration–Huge impact: Nitrate in the calcite/Eu (III) system, *Geochim. Cosmochim. Acta*, 2014, **125**, 528–538.

86 Y. Li, P. M. Kowalski, A. Blanca-Romero, V. Vinograd and D. Bosbach, Ab initio calculation of excess properties of $La_{1-x}(Ln, An)_xPO_4$ solid solutions, *J. Solid State Chem.*, 2014, **220**, 137–141.